Supramolecular Chemistry
Publication details, including instructions for authors and subscription information:
http://www.informaworld.com/smpp/title~content=t713649759

Ordered Self-assembly of a Glycine-rich Linear and Cyclic Hexapeptide: Contrasting Ultrastructural Morphologies of Fiber Growth

K. B. Joshi[a]; Sandeep Verma[a]
[a] Department of Chemistry, Indian Institute of Technology-Kanpur, Kanpur, UP, India

To cite this Article Joshi, K. B. and Verma, Sandeep(2006) 'Ordered Self-assembly of a Glycine-rich Linear and Cyclic Hexapeptide: Contrasting Ultrastructural Morphologies of Fiber Growth', Supramolecular Chemistry, 18: 5, 405 — 414
To link to this Article: DOI: 10.1080/10615800600658875
URL: http://dx.doi.org/10.1080/10615800600658875

Supramolecular Chemistry, July–August 2006 Vol. 18 (5), pp. 405–414

Taylor & Francis
Taylor & Francis Group

Ordered Self-assembly of a Glycine-rich Linear and Cyclic Hexapeptide: Contrasting Ultrastructural Morphologies of Fiber Growth

K. B. JOSHI and SANDEEP VERMA*

Department of Chemistry, Indian Institute of Technology-Kanpur, Kanpur 208016, UP, India

(Received 27 November 2005; Accepted 18 February 2006)

Self-assembly is a widely occurring phenomenon in chemistry and biology, where nanoscopic building blocks are organized to yield well-defined aggregates and supramolecular structures. One such example is ordered protein aggregation, which is primarily driven by hydrogen bonding, hydrophobic interactions and other non-covalent stabilizing factors. This report describes differing ultrastructural morphologies of a cyclic and linear hexapeptide, possessing the same amino acid sequence. Microscopic studies reveal two dissimilar pathways leading to self-assembly: one with spherical pre-fibrillar intermediate, while another one displaying spherulite-like "Maltese-cross" patterns. Detailed analysis provides crucial insight into initiation, propagation and growth of peptide fibers in two constructs.

Keywords: Peptide; Aggregation; Self-assembly; Conjugate; Ultrastructure

INTRODUCTION

The third hypervariable loop (V3 loop, residues 303–338) of HIV-1 gp120 is a crucial structural element required for its interaction with CD4 receptor and co-receptors such as CCR5 or CXCR4, which constitutes a committed first step in viral infectivity [1]. On the basis of truncated constructs, a two-site binding mechanism has been proposed for V3 loop-CCR5 interaction to facilitate viral entry into the host cells [2]. In view of this, detailed understanding of this gp120 segment has attracted considerable attention for exploring novel HIV inhibitory design paradigms [3]. A highly conserved GPGRAF hexapeptide sequence, starting at position 312, present in the V3 loop of several HIV-1 isolates is found to be critical for viral infectivity and displays a distinct conformational preference when probed in isolation by spectroscopic techniques. The hexapeptide exhibits a double-turn conformation, while its truncated tetrapeptide analog GPGR prefers a type II β-turn [4–6]. Biological role of this conserved sequence was confirmed when deletion of GPG palindrome in the hexapeptide resulted in the abrogation of HIV-1 infectivity [7], and consequently, antiviral activity of GPG tripeptide amide was described for various screens [8].

Our interest in peptide conjugates and their ordered aggregation led us to investigate tripeptide palindrome GPG and its conjugate in solid state and in solution [9]. We found that protected tripeptide affords an arrangement of stacked β-sheets, which are supported by intermolecular hydrogen bonding in the crystal lattice. However, the ordering observed in solid state was not readily translatable to assembly in solution, as confirmed by various microscopic techniques. This indicated that sheer occurrence of β-sheet orientation in solid state in this case cannot be simply extended to solution phase self-aggregation. However, we were able to enforce aggregation in GPG tripeptide palindrome by tethering it with a diamino linker to obtain a bis-conjugate **X** (Fig. 1).

Facile self-assembly of **X** in solution state provided us a hint that perhaps extended backbone hydrogen bonding plays an important role in ordered aggregation of this glycine-rich peptide. Bis-scaffold brings two GPG molecules in close proximity, thus enabling enhanced number of hydrogen bonding interactions. Two distinct arrangements of **X** can be envisaged: one where the structure remains in the

*Corresponding author. E-mail: sverma@iitk.ac.in

ISSN 1061-0278 print/ISSN 1029-0478 online © 2006 Taylor & Francis
DOI: 10.1080/10615800600658875

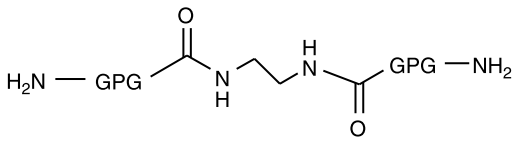

FIGURE 1 GPG bis-conjugate with a diaminoethane linker.

extended orientation and the other where it folds back on itself (Fig. 2). We decided to investigate the likelihood of these two orientations in solution by designing a pair of peptide constructs: $(GPG)_2$ and cyclo$(GPG)_2$. Both of these peptides lack flexible linker used in **X**, but contain two GPG units. Synthesis of these peptides (Scheme 1), their time-dependent aggregation and contrasting morphologies in solution-phase peptide fiber growth have been described in this report.

RESULTS AND DISCUSSION

A remarkable difference in solution phase assembly and phased growth of cyclic and linear peptides, **5** and **9**, respectively, suggest altered aggregational pathways, thus providing a crucial insight into the interactions controlling occurrence and growth of peptide seeds to persistent length fibers. These studies involved extensive microscopic analysis enabling a comment on a possible model of fiber growth.

Solution Phase Peptide Synthesis

The synthetic methodology involved standard solution-phase coupling methods via *Boc*-chemistry, active ester approach and fragment condensation. Fully deprotected cyclic hexapeptide **5** and its linear analog **9** were characterized and used for structural investigations and aging experiments. Peptide homogeneity was established by analytical HPLC, followed by FAB mass spectroscopy and CHN analysis.

CD Studies

Peptide and protein secondary structures are primarily dictated by the nature of side-chains, while it is generally believed that solution phase self-assembly of similar systems is governed by backbone interactions or via hydrogen bonding between side-chain and main chain amides. There is a general agreement that β-sheets are the dominant conformation responsible for the formation of amyloidic-type of aged peptide aggregates [10]. However, the involvement of parallel versus anti-parallel polarity of interacting β-strands in amyloid fibrils is still debated [11–14]. However, recent solid-state NMR, fluorescence and crystallographic studies suggest cross-β-spine as a probable structure of amyloid-like fibrils, where parallel β-strands are positioned perpendicular to the fiber axis [15–17].

We decided to gather CD spectral data for fresh and aged samples of **5** and **9** to ascertain starting conformations and the one which appears closer to the time of aggregation in these peptides. CD spectrum of a fresh solution of **5** was characterized by a strong negative band at 190 nm indicating a flexible, random-coil like mobile conformation (Fig. 3). An inherent flexibility in **5** has been described, however a Boltzmann-weighted CD spectrum suggests for the presence of at least one type I β-turn in this cyclic peptide [18]. Crystal structure studies indicate *trans* geometry of peptide bonds and an occurrence of two β-turns in **5** [19].

Interestingly, CD spectrum of 30 days aged solution of **5** afforded a positive band at 198 nm and a negative band at 218 nm of similar intensities, which suggested time-dependent formation of β-sheet like pattern (Fig. 3). In contrast, **9** failed to exhibit a defined conformation in fresh solutions but a hint of ordering was evident in its 21 days aged solution (Fig. 3). It could be reasoned that the cyclic peptide **5** has more conformational restrictions compared to its linear analog **9**, despite the presence of equal number of flexible glycine residues, which allows the former to achieve a defined secondary structure upon aging supported by hydrogen bonds.

Optical Microscopic Studies

Time-dependent aggregative propensities of **5** and **9** were evaluated by staining the peptide samples with Congo red dye, followed by optical microscopy. This dye binds preferentially, but not exclusively, to amyloidic protein and peptide aggregates, which appear green in color due to dye-induced birefringence when visualized under cross-polarized light [20–22]. In our case, Congo red stained samples

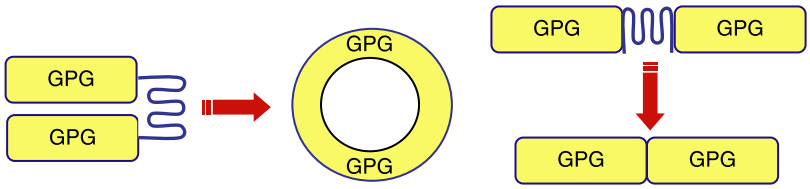

FIGURE 2 Representation of fold-back (A) and extended (B) structures and corresponding new constructs without linker as cyclic and linear peptides.

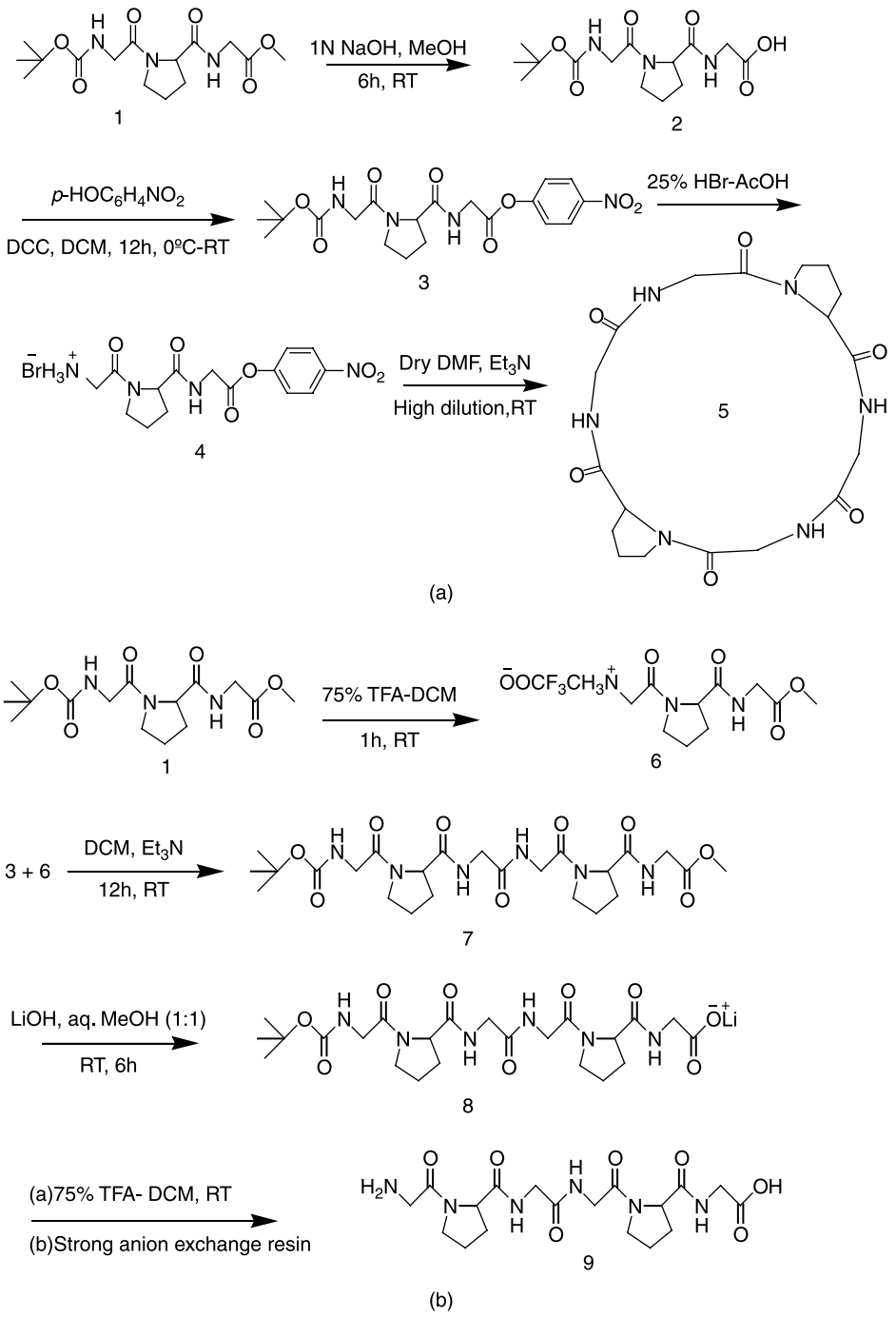

SCHEME 1 Solution-phase peptide synthesis of cyclic peptide (**5**) and linear peptide (**9**).

of **5** and **9** appeared green in color under cross-polarized light and we were able to draw significant inferences from time-course imaging of these samples.

Spherical pre-fibrillar structures were imaged in the freshly prepared aqueous solution of **5**, with observed diameters of ~2 μm (Fig. 4a). These spherical structures evolved into fibrils within 2–5 days of aging where average fibril thickness was measured as 50 μm. Further aging of the solution resulted in elongation of these fibers and after a span of 10–15 days, an average thickness of 30 μm was observed (Fig. 4c). Longer incubation for 20–30 days increased the density of fibers with a significant change in fibril cross-section to ~5 μm (Fig. 4d).

Interesting morphologies were also observed for **9** providing a hint of dissimilarity in the aggregative pathways of cyclic versus linear peptide. Fresh solution of **9** did not reveal initial assembly of peptide into spherical pre-fibrillar structures. However, 2 days aged solution of **9** exhibited appearances of two-fold symmetric "Maltese-cross" patterns which grew in

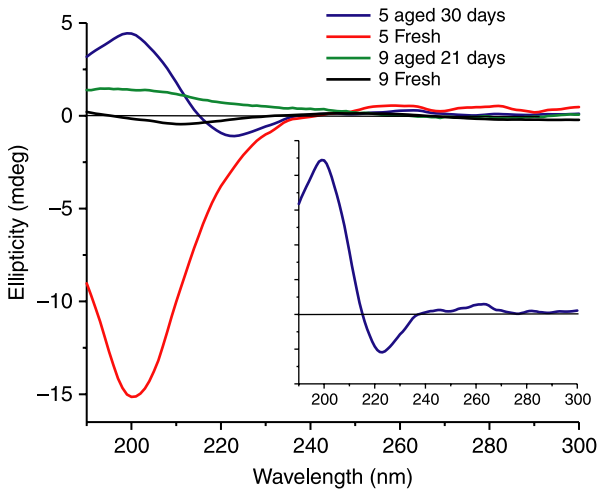

FIGURE 3 CD spectra of fresh and aged **5** and **9** in solution. Expanded spectrum of aged **5** (inset).

size upon longer incubation to 10 days, while the total number of pre-fibrillar structures decreased on prolonged incubation (Fig. 5a–c). The shape of these images suggest that aging process allows "Maltese-cross" patterned seed structures to coalesce with each other resulting in larger nuclei and that the radial growth of fibrous patterns gradually evolve from the central core eventually "ferning out" to give a dendritic fibrillar pattern (Fig. 5d–f).

In the case of insulin spherulites with "Maltese-cross" patterns, Krebs and coworkers found that core of these structures mainly comprised of non-amyloidogenic aggregate, while aligned insulin fibrils constituted the "corona" surrounding the core of spherulites offering a platform for the radial growth of fibers [23]. Analogous to this and other reported observations with varied disease states [24–26], we surmise that radial elongation of peptide fibrils from the surface of "Maltese-cross" spherulites commences once growth of precursor structures ceases in constantly aging solution of **9**. As these patterned structures are in constant contact with bulk peptide solution, a stepwise addition of precursor units with a hitherto unknown morphology permits a time-dependent, phased growth of dendritic pattern as observed in Fig. 5f.

Beside altered initial morphologies, it is also interesting to note that cyclic peptide **5** afforded rapid self-assembly. A comparison of 15 days aged solution of **5** (Fig. 4c) and that of **9** (Fig. 5d) provides remarkable difference in the kinetics of fiber growth. While **5** afforded a fully developed persistent length fibers at day 5 onwards, linear peptide was still at the level of nascent fibril growth from the core of "Maltese-cross" extinction patterns at day 15. Difference in the rate of fibril formation deserves focused investigations, but it should be emphasized that cyclic peptide **5** assembled more rapidly in

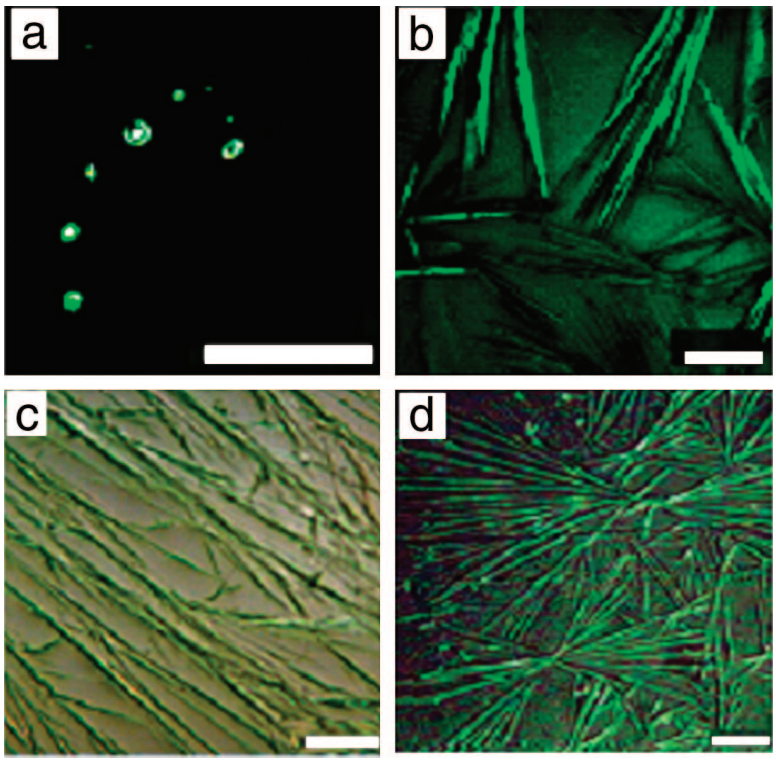

FIGURE 4 Optical micrographs of **5** self-assembly (a) Fresh solution; (b) 5 days; (c) 15 days; (d) 20 days aged solution. Scale bar for (a) and (d) 10 μm, and for (b) and (c) 100 μm.

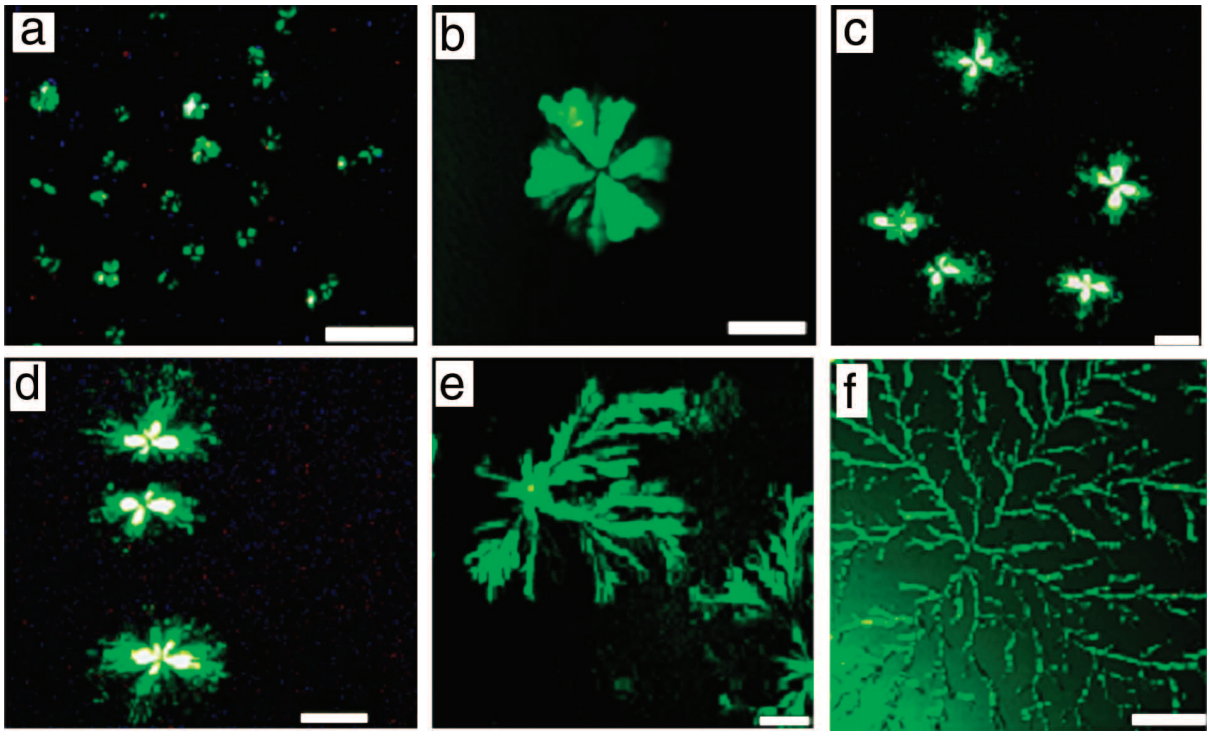

FIGURE 5 Optical micrographs of **9** self-assembly (a) 2 days; (b) 10 days; (c) 11 days; (d) 15 days; (e) 20 days; (f) 25 days aged sample. Scale bar in all pictures 200 μm.

solution compared to its conformationally labile linear counterpart.

Scanning Electron Microscopic Studies

Spherical structures, with a diameter of 2 μm, were observed in the fresh sample of **5** and it corresponded well with the optical microscopic data (Fig. 6a). After 15 days of incubation, growth of distinct fibers was evident with an average thickness of 1 μm. Further increase in the incubation time to 23 days afforded fibrils with smaller cross-section, while a month-long aging led to the formation of fibrous bundles with a large number of fibrils (Fig. 6c and d).

Interestingly, we observed radial growth of fibrils from a spherical structure in SEM micrographs for 15 days aged solution of **9** (Fig. 7). This spherulite-like morphology bears a striking resemblance to optical micrographs and confirms the presence of elongated fibrils originating from the core region. However, we were unable to discern any significant change in aggregational pattern and fibril formation in **9** even when the aging time was extended to 30 days.

Atomic Force Microscopic Studies

Freshly prepared solution of **5** revealed uniformly distributed punctuated structures, while aging of this solution at ambient temperature resulted in fiber formation (Fig. 8a and b) confirming a time-dependent aggregation and fibrillation event. However, AFM micrographs of fresh solution of **9** were poorly resolved (data not shown), but a course fibrillar network was observed after aging the sample for 21 days (Fig. 8c). AFM micrographs indicate a definite propensity of **5** and **9** to aggregate albeit with altered morphologies.

Structural Implications

Significant differences in the initial morphologies of cyclic and linear construct were evident and they were maintained till the detection of aged morphologies. Given the large number of glycine residues in these constructs, it is reasonable to assume that backbone interactions play a dominant role in aggregation. In this connection, it is relevant to mention that Gazit has recently proposed an intriguing facilitator role for aromatic-glycine motifs via bioinformatic analysis of Swiss-Prot and TrEMBL databases [27].

In the case of **5** and **9**, while glycine serves as a tightly packing amino acid spacer unit with flexible bond angle, the presence of proline residues at key positions result in conformational rigidity through a restricted range of its $\psi-\phi$ space. It is surmised that this conformational control is a contributing factor for the genesis of different starting patterns for aggregation in **5** and **9**. Such glycine-rich peptides, in the absence or presence of metal ions, have been

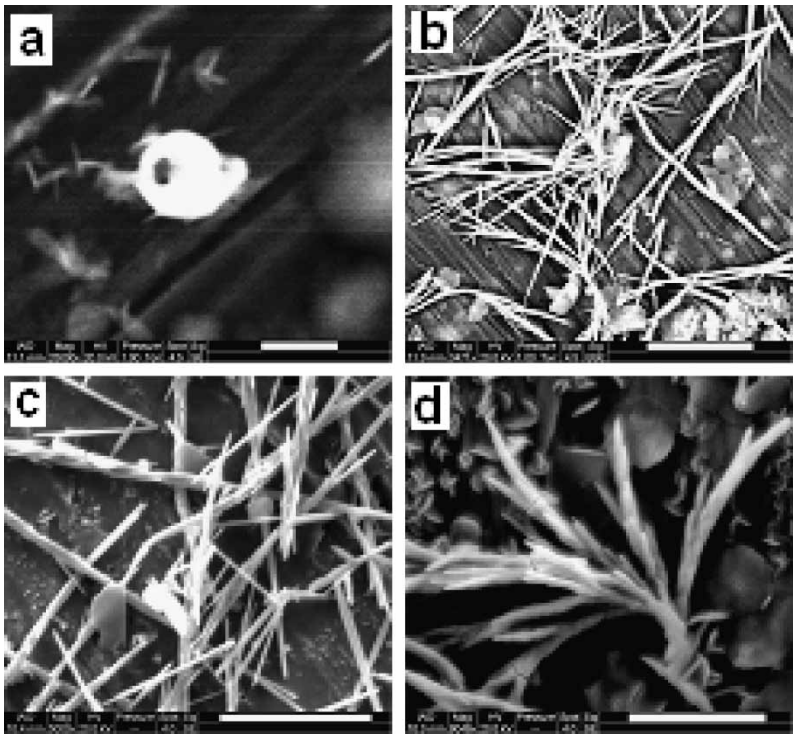

FIGURE 6 SEM images of **5** (a) Fresh; (b) 15 days; (c) 23 days; (d) 30 days aged solution. Scale bars: (a) 2, (b) and (c) 20, (d) 10 μm.

previously shown by us to self-assemble in solution leading to the formation of amyloid-like fibrous patterns upon time-dependent aging [9,28,29].

Ghadiri and coworkers have extensively applied cyclic peptides for nanotube formation where these peptides exhibit solid- and solution-phase self-assembly via extensive β-sheet networks [30,31]. In a related example, a cyclic hexapeptide homolog of gramicidin S exhibited high β-sheet content in the solution phase [32]. Similarly, ultrastructural data for

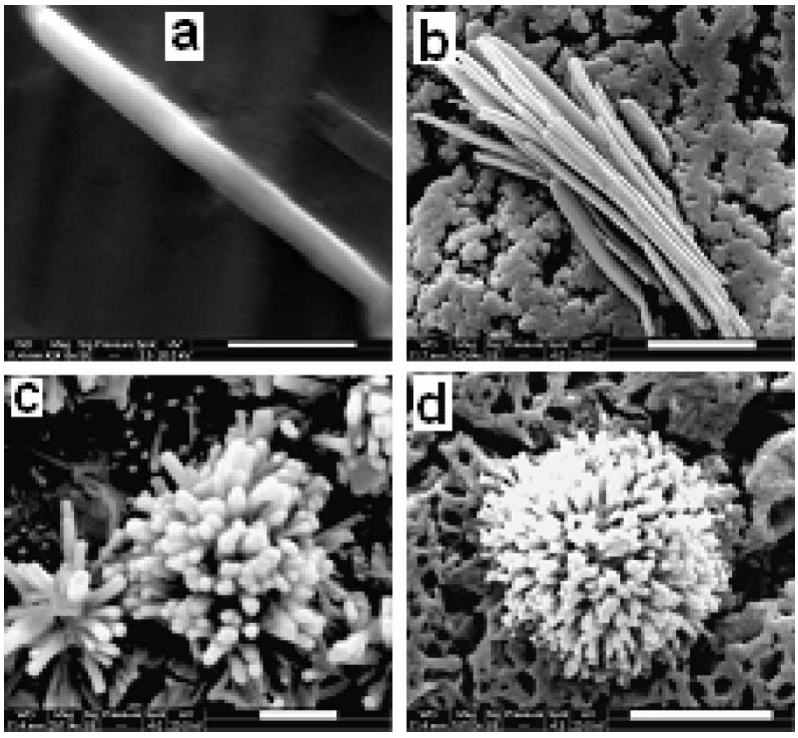

FIGURE 7 SEM images of **9** (a) 1 day aged; (b–d) 15 days aged solution of compound **9** Scale bar (a) 2.0 μm (b) 5.0 μm, (c) 2.0 μm, (d) 5.0 μm.

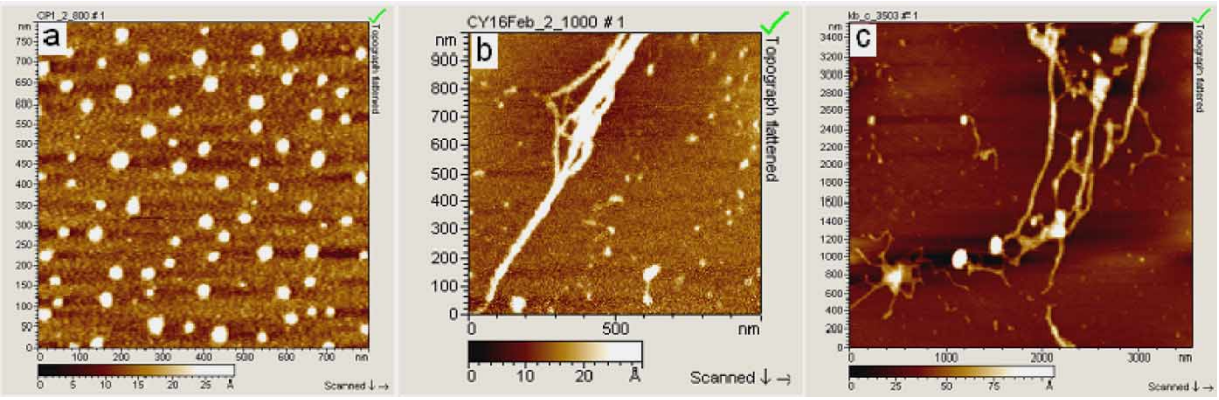

FIGURE 8 AFM micrographs: (a,b) fresh and 30 days aged **5** solution; (c) 21 days aged **9** solution.

5 suggests that this cyclic peptide quickly reaches towards intermediate conformations favoring β-sheets, aided by hydrogen bonding interactions, and stackable cyclic rings afford rapid growth of tubular structures. In contrast, delayed onset of aggregation in linear peptide **9** stems from its conformationally labile structure requiring a longer incubation to arrive at nucleating seeds which gradually grow out from the amorphous core to reveal a "ferning" dendritic pattern of fiber growth. Differing kinetics of aggregation exhibited by **5** and **9** is quite remarkable. However, it will require a detailed investigation to comment upon precise molecular basis of contrasting morphologies.

Self-aggregative propensities in peptides can be manifested by amino acids lacking interacting side-chains and the morphologies generated are perhaps a function of conformational ensembles dominating in solution. This corollary may be especially true for peptides with highly flexible backbone geometries, where thermodynamic aging leads to the stabilization of preferred solution conformation, via intra- and intermolecular hydrogen bonds, while weeding out energetically disfavored structures. We intend to pursue detailed studies of parameters responsible for peptide self-assembly in glycine-rich motifs to ascertain the role of glycine residues and its compatibility with other amino acids for aggregation.

EXPERIMENTAL SECTION

Materials and Methods

Dichloromethane, *N*,*N*-dimethylformamide, triethylamine, methanol, were distilled following standard procedures prior to use. *N*,*N*′-dicyclohexylcarbodiimide, *N*-hydroxybenzotriazole, *tert*-butyloxycarbonyl carbonate, *p*-nitrophenol, amino acids were purchased from Spectrochem (Mumbai, India) and used without further purification. ^{1}H and ^{13}C NMR were recorded on JEOL-JNM LAMBDA 400 model operating at 400 and 100 MHz, respectively. Mass spectra were recorded at Sophisticated Analytical Instrumentation Facility, Lucknow, on a JEOL SX 102/DA-6000 mass spectrometer system using Argon/Xenon (6 kV, 10 mA) as FAB gases. Elemental (C, H, N) analyses were done on Perkin-Elmer 240-C automatic elemental analyzer. All reactions were performed under nitrogen atmosphere and the solvents were evaporated under reduce pressure. The reported melting temperatures are uncorrected.

t-Butyloxycarbonyl-glycyl-prolyl-glycyl-*p*-nitrophenyl Ester (3)

Boc–GPG–OH (2.0 g, 6 mmol, 1 eq) was dissolved in dry dichloromethane (50 mL) and the solution was cooled to 0°C. To the pre-cooled solution, *p*-nitrophenol (930 mg, 6.6 mmol, 1.1 eq) was added, followed by dicyclohexylcarbodiimide (1.5 g, 7.2 mmol, 1.2 eq) with constant stirring under nitrogen atmosphere. After a span of 1 h, the reaction mixture was allowed to warm to room temperature and was further stirred for 12 h. Precipitated dicyclohexylurea was filtered off and washed with dichloromethane (2 × 10 mL). Combined filtrate was concentrated under reduced pressure and the residue was triturated with ether (3 50 mL) and filtered, to remove excess amount of *p*-nitrophenol. The product so obtained (1.9 g, 69%) was used further without any purification. $R_f = 0.6$ (9% methanol in dichloromethane), mp: 153–155°C; ^{1}H NMR: (400 MHz, $CDCl_3$, 25°C, TMS) δ (ppm) 1.44 (s, $^{t-}$Boc, 9H); 1.91 (m, 2H, Pro γ H); 2.25 (m, 2H Pro β H); 3.39–3.59 (m, 2H, Pro δ H); 3.95 (m, 2H, Gly H); 4.05 (m, 2H, Gly H); 4.29 (m, 1H, Pro α H); 5.39 (br s, $^{t-}$Boc–NH); 7.60 (appeared as br s, –NH): 7.32 (d, 2H, $J = 9.04$, aromatic H): 8.28 (d, 2H, $J = 9.04$, aromatic H); ^{13}C NMR (100 MHz, $CDCl_3$, 25°C, TMS) δ (ppm) = 23.9, 29.54, 45.94, 46.8, 58.7, 59.5, 70.6, 123.0, 125.4, 145.1, 155.5, 164.7, 168.1, 168.3, 172.0.

Anal. Calcd. for $C_{20}H_{26}N_4O_8$; C, 53.33; H, 5.82; N, 12.44%, Found C, 53.23; H, 5.61; N, 12.12%.

Cyclo-(glycyl-L-prolylglycyl)$_2$ (5)

3 (1.3 g, 2.9 mmol, 1 eq) was exposed to HBr–acetic acid (25% solution, 3.5 mL) for 1 h at room temperature. Ether (50 mL) was added to the reaction mixture and stirred for 90 min resulting in the formation of **4**. The residue so obtained was filtered and washed with hot ether (3 × 15 mL) followed by cold ether (2 × 15 mL). **4** was obtained as a white powder (0.8 g, 59%); mp: 171–173 °C (dec); ^{1}H NMR: (400 MHz DMSO-d_6, 25°C, TMS) δ (ppm) 1.90 (m, 2H, Pro γ H); 2.06 (m, 2H Pro β H); 3.44–3.56 (m, 2H, Pro δ H); 3.83 (br. s, 2H, Gly H); 4.1 (m, 2H, Gly H); 4.41 (m, 1H, Pro α H); 8.06 (br, s. –NH); 8.67 (br. s, 3H); 7.42 (m, 2H aromatic H): 8.31 (m, 2H, aromatic H); ^{13}C NMR (100 MHz, DMSO-d_6, 25°C, TMS) δ (ppm) = 23.9, 29.54, 45.94, 46.8, 58.7, 59.5, 123.0, 125.4, 145.1, 155.5, 168.1, 168.4, 172.5. Anal. Calcd. for $C_{15}H_{19}BrN_4O_6$: C, 41.78; H, 4.44; N, 12.99%, Found C, 41.52; H, 4.53; N, 13.03%. A concentrated solution of **4** (0.6 g, 1.4 mmol, 1 eq) was prepared in dry DMF (10 mL) for cyclization. It was diluted by stirring in dimethylformamide (110 ml), containing triethylamine (1.06 mL, 5.5 eq), by dropwise addition over a 3 h period at room temperature. The solution turned pale yellow in colour after this time, but the reaction mixture was further stirred 2 h, followed by the removal of solvent under reduced pressure at 60°C. The gummy residue so obtained was triturated with water and the aqueous extract was concentrated to 5 mL. This was passed through strong anion exchange resin and the eluent was concentrated to ~2 mL under reduced pressure. Acetone was added to this concentrated solution and a precipitate separated out as compound **5** (0.21 g, 37%), mp: >220°C (dec), $[\alpha]_D^t = +45°$ (*c* 0.2 in H_2O), FAB MS: (M + 1) = 423; ^{1}H NMR: (400 MHz, DMSO-d_6, 25°C, TMS) δ (ppm) 1.90–1.91 (m, 4H, Pro γ H); 2.0–2.2 (m, 4H Pro β H); 3.47–3.53 (m, 4H, Pro δ H); 3.60–3.73 (br. s, 4H, Gly H); 3.73–4.06 (m, 4H, Gly H); 4.33 (m, 2H, Pro αH); 7.59 (br.s, 2H, Gly –NH); 8.70 (br.s., 2H, Gly –NH). ^{13}C NMR (100 MHz, DMSO-d_6, 25°C, TMS) δ (ppm) = 29.56, 30.18, 47.21, 48.81, 62.15, 168.47, 175.99, 177.44. Anal. Calcd. for $C_{18}H_{26}N_6O_6$; C, 51.18; H, 6.20; N, 19.89%, Found C, 51.2; H, 6.01; N, 19.10%.

t-Butyloxycarbonyl(glycyl-L-prolyl-glycyl)$_2$ (7)

1 (1.5 g, 4.5 mmol, 1 eq) was dissolved in minimum volume of 75% trifluoroacetic acid–dichloromethane and the reaction was set aside for 1 h. After this period, excess solvent was removed and the residue was triturated with dry ether (5 × 10 mL). A white solid was obtained, which was dried under vacuum to give compound **6** (0.9 g, 89%), mp: could not be determined due to extreme hygroscopic nature of this compound. ^{1}H NMR: (400 MHz, CD_3OD, 25 °C, TMS) δ (ppm) 1.90–2.10 (m, 2H, Pro γ H); 2.19–2.22 (m, 2H Pro β H); 3.47–3.55 (m, 2H, Pro δ H); 3.71 (s, 3H, $-OCH_3$); 3.86–4.0 (m, 4H, Gly); 4.5 (m, 1H, Pro α H). ^{13}C NMR (100 MHz, CD_3OD, 25°C, TMS) δ (ppm) = 25.83, 31.22, 41.94, 42.21, 46.41, 53.04, 61.90, 166.73,171.99, 174.94. Anal. Calcd. for $C_{12}H_{18}F_3N_3O_6$; C, 40.34; H, 5.08; N, 11.76%, Found C, 40.12; H, 4.99; N, 11.52%. Condensation of two tripeptide units was achieved by reacting **3** (0.61 g 1.35 mmol, 1 eq) with **6** (0.46 g, 1.34 mmol, 1 eq) as a suspension in dry dichloromethane (25 ml) containing triethylamine (0.22 ml., 1.2 eq) and the resulting solution was set aside for 12 h at room temperature. After this time, solvent was evaporated and diethyl ether (50 mL) was added and stirred for 2 h. The residue was decanted, washed with boiling ether (5 × 10 mL) followed by cold ether (3 x 10 mL). The residue was dissolved in ethyl acetate, cooled in an ice-bath for 30 min and washed with 1N HCl (2 × 25 mL). The organic layer was dried over anhydrous sodium sulphate and concentrated under reduced pressure. Crude solid was purified by silica gel column chromatography (dichloromethane:methanol; 97:3) to yield pure compound **7** as a white solid (0.35 g, 71%), $R_f = 0.5$ (8% methanol in dichloromethane), mp: 204–206°C, FAB MS: (M + 1) = 555. ^{1}H NMR: (400 MHz $CDCl_3$, 25°C, TMS) δ (ppm) 1.37 (s, ^{t}–Boc 9H); 1.96 (br. m, 4H, Pro γ H); 2.08–2.18 (br. m, 4H, Pro β H); 3.41 (m, 4H, Pro δ H); 3.63–3.65 (overlapped signals of 5H, $-OCH_3$ & Gly H); 3.92–4.0 (overlapped signals of 6H, Gly H), 4.5 (m, 2H, Pro αH); 5.76 (br s, ^{t}–Boc N–H); 7.32 (br. s., Gly N–H); 7.40 (br. s., Gly N–H); 7.63 (br. s., Gly N–H). ^{13}C NMR (100 MHz, $CDCl_3$, 25°C, TMS) δ (ppm) = 24.71, 27.53, 28.30, 41.13, 43.01, 46.28, 52.17, 59.84, 79.76, 155.83, 168.83, 170.12, 171.13, 175.0; Anal. Calcd. for $C_{24}H_{38}N_6O_9$; C, 51.98; H, 6.91; N, 15.15%, found C, 52.01; H, 6.79; N, 15.41%.

Glycyl–L-prolyl-diglycyl-L-prolyl-glycine (9)

Lithium hydroxide (45 mg, 1.08 mmol, 6 eq) was added into an aqueous methanolic solution of **7** (100 mg, 0.18 mmol, 1 eq) and the reaction mixture was stirred for 6 h at room temperature. Solvent was evaporated under and the crude compound **8** was obtained as its lithium salt which was used further without purification. ^{1}H NMR: (400 MHz D_2O, 25°C, TMS) δ (ppm) 1.3 (s, ^{t}–Boc 9H); 1.75–1.88 (br. m, 4H, Pro γ H); 2.0–2.1 (br. m, 4H Pro β H); 3.4 (m, 4H, Pro δ H); 3.61–3.82 (overlapped signals of 6H, Gly H); 4.12 (m, 2H, Gly H), 4.32 (m, 2H, Pro αH). **8** was dissolved in 75% trifluoroacetic acid–dichloromethane (5 mL) and the reaction mixture was stirred for 1 h at room temperature. The solvent

was evaporated and the residue triturated with dry ether. The compound was dried under reduced pressure and dissolved in water (5 mL). It was passed through strong anion exchange resin to get pure **9** (55 mg, 69%). The compound was hygroscopic and prevented an accurate determination of its melting point. $[\alpha]_D^t = -8.8°$ (c 0.125 in H_2O), FAB MS: (M-1) = 439, ^{1}H NMR: (400 MHz D_2O, 25°C, TMS) δ (ppm) 1.83–1.99 (br. m, 4H, Pro γ H); 2.11–2.16 (br. m, 4H, Pro β H); 3.37–3.51(m, 6H, 4H, Pro δ H, & 2H Gly H); 3.67–3.98 (overlapped signals of 6H, Gly H); 4.34 (m, 2H, Pro αH); ^{13}C NMR (100 MHz, D_2O, 25°C, TMS) δ (ppm) = 23.4, 25.0, 25.4, 25.5, 33.0, 41.4, 41.6, 42.3, 47.3, 47.6, 61.1, 61.7, 162.5, 162.8, 163.2, 163.5, 166.0, 166.7. Anal. Calcd. for $C_{18}H_{28}N_6O_7$; C, 49.08; H, 6.41; N, 19.08%, Found C, 48.99; H, 6.16; N, 19.00%.

Optical Microscopy

Congo red (3 μM dye in 100 mM NaCl) was added to aged solution of peptide conjugates and the mixture was left for 6 h at room temperature. 50 μL of this solution was transferred on to glass slides and dried to make a thin film, then viewed under optical microscope (Zeiss) with cross-polarized light (magnification 50 ×). Images were obtained by using Image-Pro Plus software.

Atomic Force Microscopy

Test peptides (1 mM) were incubated for 0–30 days in water. 10μL of this solution was transferred on to freshly cleaved mica at appropriate time intervals and uniformly spread with the aid of a spin-coater operating at 200–500 rpm (PRS-4000). The deposited samples were imaged with atomic force microscope (Molecular Imaging, USA), operating under Acoustic AC mode (AAC), with the aid of a cantilever (NSC 12 (c) from Mikro Masch). The force constant was 0.6 N/m, while the resonant frequency was 150 kHz. The images were taken in air at room temperature with a scan speed of 1.5–2.2 lines/sec. Data acquisition was done with PicoScan 5® software, while the data analysis was done with the aid of visual SPM.

Scanning Electron Microscopy

SEM analysis was performed on FEI QUANTA 200 microscope with a tungsten filament gun. Image was recorded for compounds **5** and **9** at WD 10.6 mm, magnification 9000X–40,000X, HV 20 kV, Spot 5.0, Sig SE. **5** and **9** were dissolved in distilled and double deionized water and aged for 0–30 days. A few drops of fresh and incubated solutions were taken and placed on copper stubs inside the microscope chamber of an FEI QUANTA 200 microscope. The samples were left to equilibrate at 25°C. The chamber sealed and evacuated to ~1.00 Torr.

CD Spectroscopy

CD spectra were recorded at 25°C under a constant flow of nitrogen on a JASCO-810 Spectropolarimeter, which was calibrated with an aqueous solution of (+)-ammonium D-camphor sulphate. Experimental measurements were carried out in water and at different pH values by using a 1 mm path length cuvette. The CD spectra were recorded in the UV region (190–300 nm). The spectrum represents an average of 5–8 scans and the CD intensities are expressed in mdeg.

Acknowledgements

KBJ thanks IIT-Kanpur for a graduate fellowship. Authors thank Prof. Ashutosh Sharma, Chemical Engineering, and ACMS, IIT-Kanpur, for microscopic facilities. This work is supported by a Swarnajayanti Fellowship to SV from Department of Science and Technology, India.

References

[1] LaRosa, G. J.; Davide, J. P.; Weinhold, K.; Waterbury, J. A.; Profy, A. T.; Lewis, J. A.; Langlois, A. J., *et al. Science* **1990**, *249*, 932.
[2] Cormier, E. G.; Dragic, T. *J. Virol* **2002**, *76*, 8953.
[3] Sirois, S.; Sing, T.; Chou, K. C. *Curr. Protein Pept. Sci.* **2005**, *6*, 415.
[4] Ghiara, J. B.; Stura, E. A.; Stanfield, R. L.; Profy, A. T.; Wilson, I. A. *Science* **1994**, *264*, 82.
[5] Gunasekaran, K.; Ramakrishnan, C.; Balaram, P. *Int. J. Pept. Protein Res.* **1995**, *46*, 359.
[6] Catasti, P.; Bradbury, E. M.; Gupta, G. J. *Biol. Chem.* **1996**, *271*, 8236.
[7] Su, J.; Palm, A.; Wu, Y.; Sandin, S.; Hoglund, S.; Vahlne, A. *AIDS Res. Hum. Retroviruses* **2000**, *16*, 37.
[8] Su, J.; Andersson, E.; Horal, P.; Naghavi, M. H.; Palm, A.; Wu, Y. -P.; Eriksson, K.; Jansson, M.; Wigzell, H.; Svennerholm, B.; Vahlne, A. *J. Hum. Virol.* **2001**, *4*, 1.
[9] Prasad, K. K.; Purohit, C. S.; Jain, A.; Sankararamakrishnan, R.; Verma, S. *Chem. Commun.* **2005**, 2564–2566.
[10] Sunde, M.; Serpell, L. C.; Bartlam, M.; Fraser, P. E.; Pepys, M. B.; Blake, C. C. *J. Mol. Biol.* **1997**, *273*, 729.
[11] Balbach, J. J.; Petkova, A. T.; Oyler, N. A.; Antzutkin, O. N.; Gordon, D. J.; Meredith, S. C.; Tycko, R. *Biophys. J.* **2002**, *83*, 1205.
[12] Fay, N.; Redeker, V.; Savistchenko, J.; Dubois, S.; Bousset, L.; Melki, R. *J. Biol. Chem.* **2005**, *280*, 37149.
[13] Petty, S. A.; Decatur, S. M. *Proc. Natl. Acad. Sci. USA* **2005**, *102*, 14272.
[14] Makin, O. S.; Atkins, E.; Sikorski, P.; Johansson, J.; Serpell, L. C. *Proc. Natl. Acad. Sci. USA* **2005**, *102*, 315.
[15] Ritter, C.; Maddelein, M. L.; Siemer, A. B.; Luhrs, T.; Ernst, M.; Meier, B. H.; Saupe, S. J.; Riek, R. *Nature* **2005**, *435*, 844.
[16] Nelson, R.; Sawaya, M. R.; Balbirnie, M.; Madsen, A. O.; Riekel, C.; Grothe, R.; Eisenberg, D. *Nature* **2005**, *435*, 773.
[17] Krishnan, R.; Lindquist, S. L. *Nature* **2005**, *435*, 765.
[18] McFarlane, K. J.; Humbert, M. M.; Thomasson, K. A. *Int. J. Pept. Protein Res.* **1996**, *47*, 447.
[19] Kostansek, E. C.; Thiessen, W. E.; Schomburg, D.; Lipscomb, W. N. *J. Am. Chem. Soc.* **1979**, *101*, 5811.
[20] Nilsson, M. R. *Methods* **2004**, *34*, 151.

[21] Khurana, R.; Uversky, V. N.; Nielsen, L.; Fink, A. L. *J. Biol. Chem.* **2001**, *276*, 22715.
[22] Lyons, R. P.; Atkins, W. M. *J. Am. Chem. Soc.* **2001**, *123*, 4408.
[23] Krebs, M. R. H.; Macphee, C. E.; Miller, A. F.; Dunlop, I. E.; Dobson, C. M.; Donald, A. M. *Proc. Natl. Acad. Sci. USA* **2004**, *101*, 14420.
[24] Jin, L. W.; Claborn, K. A.; Kurimoto, M.; Geday, M. A.; Maezawa, I.; Sohraby, F.; Estrada, M.; Kaminksy, W.; Kahr, B. *Proc. Natl. Acad. Sci. USA* **2003**, *100*, 15294.
[25] Basak, S.; Ferrone, F. A.; Wang, J. T. *Biophys. J.* **1988**, *54*, 829.
[26] Gardner, G. C.; Terkeltaub, R. L. *J. Rheumatol.* **1989**, *16*, 394.
[27] Gazit, E. *Bioinformatics* **2002**, *18*, 880.
[28] Madhavaiah, C.; Verma, S. *Bioorg. Med. Chem. Lett.* **2005**, *13*, 3241.
[29] Madhavaiah, C.; Verma, S. *Chem. Commun.* **2004**, 638.
[30] Clark, T. D.; Buriak, J. M.; Kobayashi, K.; Isler, M. P.; McRee, D. E.; Ghadiri, M. R. *J. Am. Chem. Soc.* **1998**, *120*, 8949–8962.
[31] Kobayashi, K.; Granja, J. R.; Ghadiri, M. R. *Angew. Chem. Int. Ed. Engl.* **1995**, *34*, 95–98.
[32] Gibbs, A. C.; Kondejewski, L. H.; Gronwald, W.; Nip, A. M.; Hodges, R. S.; Sykes, B. D.; Wishart, D. S. *Nat. Struct. Biol.* **1998**, *5*, 284–288.